Band-Attention Modulated RetNet for Face Forgery Detection

Zhida Zhang[1,2], Jie Cao[2], Wenkui Yang[1], Qihang Fan[1,2], Kai Zhou[3], and Ran He[1,2]

[1] University of Chinese Academy of Sciences, Beijing, China
[2] MAIS & CRIPAC, Institute of Automation, Chinese Academy of Sciences, Beijing, China
[3] Meituan, Beijing, China
zhida.zhang@cripac.ia.ac.cn, jie.cao@cripac.ia.ac.cn, yangwenkui20@mails.ucas.ac.cn, fanqihang.159@gmail.com, zhoukai03@meituan.com, rhe@nlpr.ia.ac.cn

Abstract. The transformer networks are extensively utilized in face forgery detection due to their scalability across large datasets. Despite their success, transformers face challenges in balancing the capture of global context, which is crucial for unveiling forgery clues, with computational complexity. To mitigate this issue, we introduce Band-Attention modulated RetNet (**BAR-Net**), a lightweight network designed to efficiently process extensive visual contexts while avoiding catastrophic forgetting. Our approach empowers the target token to perceive global information by assigning differential attention levels to tokens at varying distances. We implement self-attention along both spatial axes, thereby maintaining spatial priors and easing the computational burden. Moreover, we present the adaptive frequency Band-Attention Modulation mechanism, which treats the entire Discrete Cosine Transform spectrogram as a series of frequency bands with learnable weights. Together, BAR-Net achieves favorable performance on several face forgery datasets, outperforming current state-of-the-art methods.

Keywords: Face Forgery Detection · Retentive Network · Band Attention Modulation

1 Introduction

Deep learning models have the ability to generate and synthesize hyper-realistic images, and these forgeries, often referred to as "deepfakes", can be exploited for malicious purposes, raising serious trust and security concerns in our society. Their potential misuse is a cause for concern. Therefore, the development of effective forgery detection methods has become a crucial task.

In some of the early work [1] [30] [33], face forgery detection was treated as a binary classification problem aimed at learning the decision boundary between real and generated faces. Most previous methods [5] [29] [46] are constructed

based on Convolutional Neural Networks (CNNs) and have achieved good performance for intra-dataset evaluation. However, due to the image-specific generalization bias caused by the limited receptive field of CNNs, these methods usually have poor generalization performance on unseen datasets.

The self-attention mechanism in Transformer [43] allows the model to consider the entire content of the input sequence at various locations simultaneously, which enables it to capture long-range dependencies within the sequence. This mechanism is also well suited for processing image data since the relationships between elements (pixels) in an image are often global and complex. With the successful application of transformer in various visual tasks, some researchers have tried to use pure visual transformers [9] or combine the self-attention mechanism in the transformer architecture with CNNs [45] [44] [53] for face forgery detection. However, although Transformer is excellent at handling global dependencies, it faces computational and memory consumption challenges when processing large-scale image data due to its fully-connected nature. In addition, the self-attention mechanism of pure visual transformers emphasizes coarse granularity but is not good at capturing fine-grained feature details, and it is precisely these subtle fine-grained artifacts that are important in face forgery detection [51].

Recently, a novel model known as the Retentive Network (RetNet) [39] has emerged within the field of natural language processing. By leveraging a unique retention mechanism, RetNet successfully integrates the strengths of recurrent neural networks and Transformer architectures, delivering training parallelism, cost-efficient inference, and superior performance. The core of the retention mechanism is a time decay matrix, which correlates with sequence distances, thereby providing a temporal prior that enhances the model's comprehension of sequential information in the text.

Drawing inspiration, we extend the network structure that applies to unidirectional, one-dimensional text to a bidirectional format, effectively expanding the one-dimensional time decay matrix into a two-dimensional spatial matrix based on Manhattan distance. The resulting model is termed Two-dimensional RetNet (2D-RetNet). Within the spatial matrix, attention scores for a target token decay with increasing distance from surrounding tokens. This characteristic empowers the target token to perceive global information by assigning varying degrees of attention to tokens at different distances. We then incorporate this spatial decay matrix to introduce explicit spatial information prior to the visual trunk. This novel self-attention mechanism, named Forgery Detection Self-Attention (FDSA), is inspired by RetNet and utilizes Manhattan distance as an explicit spatial prior. However, the global modeling of self-attention imposes a significant computational burden, and the decomposition rooted in RetNet disrupts the spatial decay matrix, rendering it unsuitable for FDSA. In response to this challenge, we apply self-attention along both spatial axes to decompose the image, which preserves the spatial priors in both the self-attention and spatial decay matrices. This approach enables us to model global information without compromising the integrity of the spatial decay matrices.

Following the development of our 2D-RetNet and its application in the spatial domain, we further exploit the complementary frequency domain information, which is considered effective in amplifying specific artifacts introduced during face manipulation. However, in previous investigations, the predominant methodology relies mainly upon hand-crafted band-pass filters. This approach provides merely a rudimentary dichotomy for each coarse-grained band: either permitting their transmission or subjecting them to filtration, and may consequently inherently limit adaptability and robustness.

To enhance the flexibility and performance of our forgery detection system, we propose our adaptive front-end frequency Band Attention Modulation (BAM) mechanism. After extracting frequency information via Discrete Cosine Transformation (DCT), the low-frequency component occupies the top-left corner of the spectrogram, while the higher component lies on the bottom-right corner. Thus, BAM views the entire DCT spectrogram as a stack of frequency bands along the anti-diagonal direction and adaptively adjusts the weights of these bands. In conjunction with our 2D-RetNet, this frequency-based modulation approach allows us to perform without much performance degradation even on the higher compression forged image dataset (FF++c40) compared to the lower compression level dataset (FF++c23).

Finally, the integration of our 2D-RetNet and BAM forms the Band-Attention modulated RetNet (BAR-Net), a more comprehensive and more robust solution for face forgery detection. In our experiments, BAR-Net improves the discrimination performance on currently popular forgery image datasets, surpassing the performance of current state-of-the-art methods, and providing a novel approach to face forgery detection.

2 Related Work

Face Forgery Detection has made tremendous progress in recent years, with a series of models have been proposed to meet practical applications. ProGAN [11] and StarGAN [4] are capable of generating visually extremely realistic face images, which are difficult to distinguish the authenticity with the naked eye. Therefore, McCloskey [26] proposed that the color image of the GAN-generated image differs from the real image in color distribution, and classification is performed by constructing color features and using a support vector machine. Liu [23] proposed that there are texture differences between the generated image and the real image, and used the Gram matrix to represent the texture. Xuan [49] proposed that Gaussian blending and Gaussian noise preprocessing of images can improve the representation and generalization ability of neural networks.

For face swapping and face reconstruction techniques, Sun [52] proposed a spliced tampered forged image detection method based on bias color estimation. Rössler et al. directly used the Xception [33] network structure to train a binary classification on a large-scale forged face dataset network, demonstrating that using only images of face regions to participate in training outperforms using whole images. Meanwhile, the higher the compression level of the forged images

and videos, the lower the detection correctness of the classifier. Dang [7] introduced an attention mechanism to prompt the model to focus on more meaningful information and trained on the fake dataset, outputting both the classification results and the heat maps of the modified regions. In addition, Biobehavior-based approaches have been proposed to detect authenticity (e.g., blinking [24], head movements [14], lip movements [15]).

Although all existing algorithms have made some progress, more in-depth forgery algorithms are still possible in the future. Unlike existing networks, we use RetNet as a backbone for the first time and find its potential in visual forgery.

3 Method

In this section, we present a comprehensive overview of our model. In Section 3.1, we briefly review the principles and methodologies underpinning RetNet. Subsequently, in Section 3.2, we extend RetNet to a 2D-RetNet framework tailored for image processing, which effectively extracts features from images. Next, in Section 3.3, we introduce BAM, an attention mechanism that dynamically modulates each frequency component within the frequency domain. Finally, in Section 3.4, we introduce our integrated pipeline, BAR-Net, designed for face forgery detection, which consists of a front-end BAM component and a 2D-RetNet module, as illustrated in Fig. 1.

3.1 Preliminary

Retentive Network. Retentive Network (RetNet) is a strong architecture for large language models. This work proposes a retention mechanism that has a dual form of recurrence and parallelism, which can train the models in a parallel way while recurrently conducting inference. For a sequence modeling problem that maps $v\left(n\right) \mapsto o\left(n\right)$ through states s_n, they deduce:

$$o_n = \sum_{m=1}^{n} \gamma^{n-m} \left(Q_n e^{in\theta}\right) \left(K_m e^{im\theta}\right)^{\dagger} v_m \tag{1}$$

where o_n, v_m denote $o(n), v(m)$, γ is a scalar, $\dagger$ is the conjugate transpose. The formulation is easily parallelizable. The parallel representation of retention is written as:

$$Q = (XW_Q) \odot \Theta, K = (XW_K) \odot \bar{\Theta}, V = XW_V \tag{2}$$

$$\Theta_{\mathrm{n}} = e^{in\theta}, D_{nm} = \begin{cases} \gamma^{n-m}, & n \geq m \\ 0, & n < m \end{cases} \tag{3}$$

$$\text{Rentention}(X) = (QK^{\intercal} \odot D)V \tag{4}$$

where W_Q, W_K, W_V are learnable matrices, $\bar{\Theta}$ is the complex conjugate of Θ, and $D \in \mathbb{R}^{|x| \times |x|}$ combines causal masking and exponential decay along relative

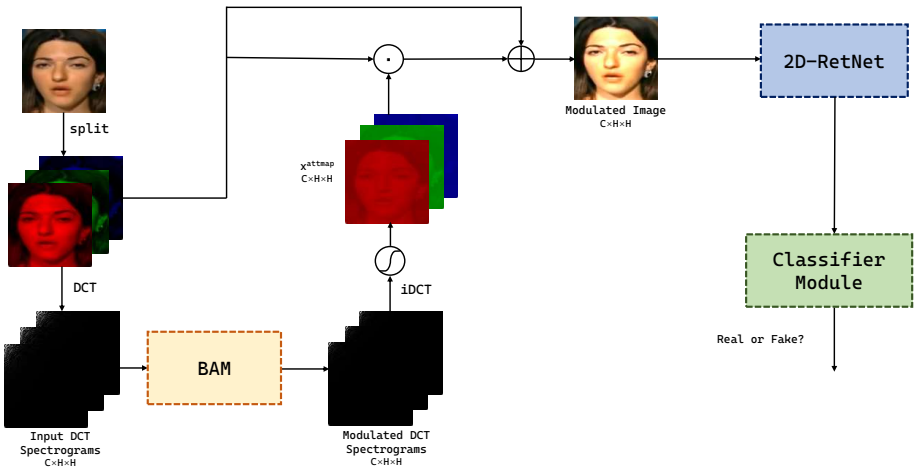

Fig. 1: Overview diagram of our BAR-Net. The original DCT spectrograms serve as the inputs to the front-end Band Attention Modulation (BAM), yielding modulated spectrograms. Subsequently, through inverse Discrete Cosine Transform (iDCT) and Sigmoid, these spectrograms are converted into x^{attmap}, which are employed as attention maps for modulating spatial information. The modulated images are finally processed by our 2D-RetNet to extract features for forgery detection.

distance as one matrix, which symbolizes relative distances in a one-dimensional sequence and brings in explicit time before the textual data.

3.2 Two-dimensional Retentive Network (2D-RetNet)

Similar to ViT, In model design we follow the original RetNet as closely as possible. However, there are two obvious problems with the application of RetNet to computer vision. First, retention carries causal properties information, whereas pictures cannot consider only unidirectional information; second, retention deals with one-dimensional data, whereas pictures are two-dimensional.

For the first problem, we first extend the original unidirectional information symmetry of retention into a bidirectional state, expressed as follows

$$D_{nm}^{ex} = \gamma^{|n-m|} \tag{5}$$

$$\text{Retention}(X) = (QK^{\intercal} \odot D_{nm}^{ex})V \tag{6}$$

After the extension of Eq. (6), retention already can be modeled in both directions, but this ability is still limited to the one-dimensional level, and we need to extend the one-dimensional retention into a two-dimensional retention.

Similar to a one-dimensional line, each pixel of a two-dimensional image also has a unique coordinate (x_i, y_i), and for the $n-th$ token, we denote its coordinate

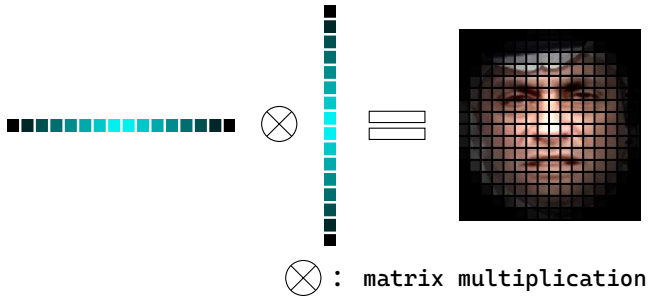

Fig. 2: Attentional decay in FDSA: we apply self-attention along both spatial axes to decompose the image, which preserves the spatial a priori information in both the self-attention and spatial decay matrices. the higher brightness is also the place where our image focuses more.

by (x_n, y_n).To adapt to the new two-dimensional coordinates, we modify each element of matrix D to the Manhattan distance of the corresponding token pair at its respective position, completing the conversion from 1D to 2D attenuation coefficients. The new matrix D transfers to Eq. (7):

$$D_{nm}^{2D} = \gamma^{|x_n - x_m| + |y_n - y_m|} \tag{7}$$

The use of the gating function in retention empowers RetNet to be computationally flexible in a variety of ways and adaptable to parallel training and recursive inference processes. However, the nature of forensics is a binary classification task, and this gating function does not improve the results but rather introduces additional parameters and computational complexity. We use sigmoid to endow the model with nonlinearity, and our Forgery-Detection Self-Attention can be expressed as:

$$\text{FDSA}(X) = (\text{Sigmoid}(QK^{\intercal}) \odot D_{nm}^{2D})V \tag{8}$$

Considering the computational cost problem, we divide the image into two axes, and the shape of the feeling field of each token is shown in Fig. 2, the higher brightness is also the place where our image focuses more.

3.3 Band Attention Modulation (BAM)

To surpass conventional hand-crafted high-pass filters, such as merely cutting off the lowest 1/8 component of a DCT spectrogram, BAM operates by transforming images into frequency spectrograms via DCT, wherein coefficients from similar

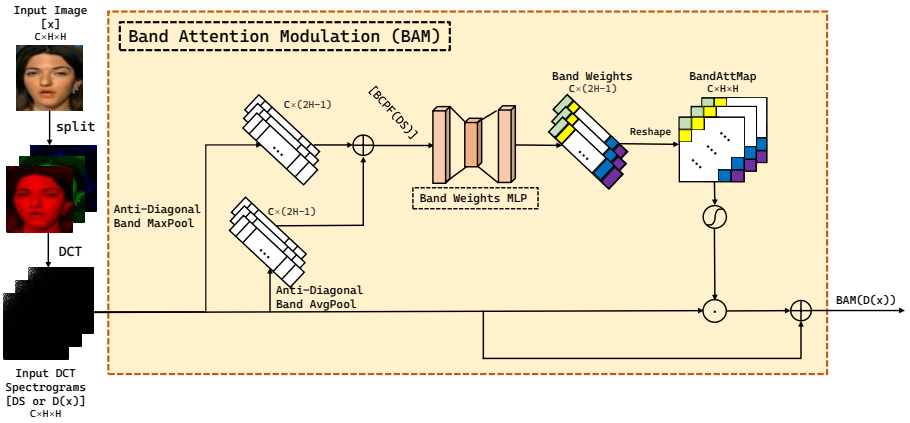

Fig. 3: Band Attention Modulation (BAM). BAM takes the DCT spectrograms as its inputs, and coefficients on the same anti-diagonal are viewed as frequency components on the same band. Global Max-Pooling (GMP) and Global Average-Pooling (GAP) are then both employed to extract the features out of each band. Following this, two fully connected layers are employed to calculate these band weights, which are later reshaped to match the dimensions of the input spectrograms. The reshaped $BandAttMap$ is then utilized for attention modulation on the original DCT spectrograms.

frequency components along horizontal and vertical directions are grouped into the same frequency band. This approach allows BAM to dynamically adjust the weights associated with these band channels to adapt to the input data. Fig. 3 illustrates the diagram of the entire BAM.

Specifically, let $x \in \mathbb{R}^{3\times H\times W}$ denotes a 3-channel RGB image, where H and W are respectively the height and the width of the input image. In BAM, H and W are supposed to be equal, necessitating a square input configuration. On this premise, BAM views different fine-grained frequency bands along the anti-diagonal direction (from bottom-left to top-right) in the DCT spectrogram as different channels.

In our implementation, we take the minimum band channel granularity and set the bandwidth to 1, i.e., each band channel among the total $(2H-1)$ anti-diagonals is allocated one single channel weight. Inspired by CBAM [48], Global Max-Pooling (GMP) and Global Average-Pooling (GAP) values of frequency band channels are combined via addition or concatenation. Thus, our feature extraction process for each frequency band channel can be formulated as:

$$\mathrm{BCPF}(DS) = \mathrm{GMP}[\mathrm{AntiDiags}(DS)] + \mathrm{GAP}[\mathrm{AntiDiags}(DS)] \tag{9}$$

where DS represents the input monochrome DCT spectrogram, $\mathrm{BCPF}(\cdot)$ means **b**and **c**hannel **p**ooling **f**eatures, and $\mathrm{AntiDiags}(DS)$ refers to a tensor with a

length of $(2H-1)$, where each element is a band channel tensor, containing different numbers of coefficients from the same anti-diagonal of the original DS.

Notice that the lengths of these heterogeneous band channels follow arithmetic progressions with a tolerance of 2, extending until reaching the maximum H, and then contracting from H back to 1 with a tolerance of -2. This heterogeneity in lengths across these band channels, however, is smoothed out by GMP and GAP later, yielding monochrome BCPF(DS) in the shape of $\mathbb{R}^{(2H-1)}$.

Afterward, BCPF(DS) is transmitted through two fully connected layers while preserving its shape to learn the attention weights of diverse band channels. Then during reshaping, these weights are copied along the anti-diagonal direction to restore the original shape, forming $BandAttMap$, where each color refers to one single weight for one band channel, as shown in Fig. 3. Finally, the original DCT spectrogram is modulated by normalized Sigmoid($BandAttMap$) through the residual connection. In summary, the whole BAM process is formulated as:

$$BandAttMap = \text{Reshape}\{2 - \text{FCLayers}[\text{BCPF}(DS)]\} \tag{10}$$

$$\text{BAM}(DS) = \text{Sigmoid}(BandAttMap) \odot DS + DS \tag{11}$$

3.4 Band-Attention modulated RetNet (BAR-Net)

As shown in Fig. 1, following frequency modulation, the frequency domain information conveyed by the spectrogram is transformed back to the spatial domain via iDCT. We note that legitimate pixel color values may not instantly be guaranteed after conducting iDCT on the modulated spectrogram, since iDCT here is employed solely to restore the corresponding spatial relationship of pixels, rather than enhancing artifacts in visualizations. Afterward, the result obtained in the frequency domain is further utilized as the spatial attention map after Sigmoid to modulate the original input image in the spatial domain. In summary, the total modulation process can be formulated as:

$$x^{attmap} = \text{Sigmoid}(\mathcal{D}^{-1}\{\text{BAM}[\mathcal{D}(x)]\}) \tag{12}$$

$$x' = x^{attmap} \odot x + x \tag{13}$$

where $\odot$ denotes the Hadamard product, while $\mathcal{D}(\cdot)$ and $\mathcal{D}^{-1}(\cdot)$ denote respectively DCT and iDCT. $\mathcal{D}(x)$ in Eq. (12) is an alias for DS in Eq. (9), Eq. (10) and Eq. (11). As a consequence, x' represents the resultant image modulated by x^{attmap}, wherein any artifacts present within specific frequency components, if they do exist, are anticipated to be accentuated.

Finally, we feed the resultant image into a 2D-RetNet, which is then subjected to a simple classification module for forgery detection.

4 Experiment

4.1 Dataset

To evaluate the capability of our proposed method, we build different benchmarks based on three popular deepfake databases FaceForensics++ (FF++) [33],

Celeb-DF [21], and Deepfake Detection Challenge (DFDC) [8]. In this paper, we divide the experiments into three parts: intra-dataset, unseen datasets (cross-dataset), and unseen manipulations (cross-manipulation).

Intra-Dataset Evaluation. FaceForensics++ (FF++) is adopted with two challenging quality levels, i.e., High Quality (C23) and Low Quality (C40). FF++ consists of 1,000 original videos and 4,000 corresponding dummy videos generated by four typical processing methods. We use 720 training videos, 140 validation videos, and 140 test videos out of every 1000 videos following the methodology [28]. The number of frames in each video ranges from about 300 to 699, so we extract about 400 frames from each video for test evaluation. However, only 20 frames are selected for training.

Celeb-DF includes 590 real videos and 5,639 high-quality fake videos which are crafted by the improved DeepFake algorithm. DFDC is a large-scale dataset that contains 128,154 facial videos of 960 subjects. For the Celeb-DF and DFDC datasets, we use a similar approach for testing.

Unseen Datasets Evaluation. We train the proposed method on FF++ and then test it on two unseen datasets, including Celeb-DF, and DeepFake Detection Challenge (DFDC).

Unseen Manipulations Evaluation. We perform these experiments on the FF++ dataset with four forgery methods, including two computer graphics methods (Face2Face (FF) [42] and FaceSwap (FS) [17]) and two learning-based methods (DeepFakes (DF) [16] and NeuralTextures (NT) [41]). Considering the significant differences in results achieved by each forgery method, we use these different methods as a basis for dividing the source and target domains. In particular, we train with three forgeries and tested with the remaining one.

4.2 Experimental Setup

Evaluation Metrics. To evaluate our method, we use the Accuracy score (Acc) and Area Under the Receiver Operating Characteristic Curve (AUC) as our evaluation metrics. To ensure fair comparisons, the results of the compared methods are extracted from their papers or reproduced from other papers.

Implementation Details. We use the DLIB [34] for face extraction and alignment. The input shape of images is resized to 224×224 with random erasing as a data augmentation technique. We use the Adam optimizer for optimizing the network with $\beta_1 = 0.9$ and $\beta_2 = 0.99$. The learning rate for the training phase is set to 0.0001 for the first epoch.

4.3 Experimental Results

Intra-Dataset Evaluation. In this section, we first compare our method with state-of-the-art face forgery detection respectively on the widely used dataset FF++ of High Quality (C23) and Low Quality (C40). As shown in Tab. 1, our models are consistently ahead of the others by a relatively large margin. For

Table 1: Comparison Against State-of-the-Art Approaches on the **Intra-Dataset (IL: Image-Level)**: For each frame in the dataset, the authenticity is independently determined and the results are compared at the image-level. The top three performances are highlighted in red, green, and blue, respectively.

Method	FF++c40		FF++c23	
	AUC	Acc	AUC	Acc
Steg. Features [10]	55.98	-	70.97	-
Cozzolino et al. [5]	58.69	-	82.97	-
Bayar & Stamm [2]	66.86	-	82.97	-
Rahmouni et al. [32]	70.47	-	83.10	-
MseoNet [1]	-	70.47	-	83.10
Xception [33]	81.76	80.32	94.86	92.39
SPSL [22]	82.82	81.57	95.32	91.50
F^3-Net [31]	87.22	84.53	97.80	93.12
M2TR [45]	87.97	85.09	97.84	93.22
LiSiam [44]	89.02	86.50	-	-
F^2Trans-B [28]	89.91	87.20	99.24	96.60
Ours	**93.19**	**89.63**	**99.32**	**97.02**

example, compared with the state-of-the-art method F^2Trans, the AUC of our model exceeds it by 2.57% in dataset FF++c40, and this performance gain is also observed in Acc.

As a special note, many types of studies report video-level performance metrics, even though their models are image-based. Our model also targets image-based forgery detection. For a fair comparison, in addition to the image-level-based metrics shown Tab. 1, we also adopt the image-based video-level (IVL) approach to compute the video-level results during the testing phase. Specifically, we compute the video-level predictions by averaging the scores of the frame sequences. The experimental results are shown in Tab. 2. Because of the data distribution problem in the FF++ dataset (1:4 ratio of true to false), we usually consider the AUC to be more informative than the Acc, and we achieve the highest value or get close to it, both in terms of Image-Level and Image-based Video-Level evaluations. In particular, our model's results for low-quality images (FF++c40) improve considerably compared to previous models.

In addition, our model also does well in high-definition image detection. In the celeb dataset, a relatively simple one, our AUC reaches **100%**. As for the DFDC dataset, we also obtain a significant improvement.

Unseen Datasets Evaluation. In the real world, many manipulated faces are unknown, i.e. they are generated by anonymous tampering using unknown source data. Therefore, in this section, we conduct a cross-dataset generalization experiment where our model uses training and testing sets from different datasets, i.e., we use FF++c23 or FF++c40 for training and then test it on the

Table 2: Comparison of Performance Against State-of-the-Art Approaches Using the **Intra-Dataset (IVL: Image-based Video-Level)**: For each video authenticity verification within the dataset, results are compared to those obtained using the image-based video-level method. The top three performances are highlighted in red, green, and blue respectively.

Method	FF++c40		FF++c23		Celeb-DF		DFDC	
	AUC	Acc	AUC	Acc	AUC	Acc	AUC	Acc
Xception [33]	89.30	86.86	94.80	93.86	99.73	97.90		
F^3-Net [31]	93.30	90.43	98.10	97.52	98.93	95.95	-	-
M2TR [45]	92.46	88.71	99.19	96.14	-	-	-	-
LiSiam [44]	93.99	88.86	-	-	-	-	-	-
ITA-SIA [36]	93.45	90.23	99.35	97.64	99.94	98.59	91.33	81.20
DisGRL [35]	95.19	91.27	99.48	97.69	99.91	98.71	92.50	82.35
F^2Trans-B [28]	94.04	90.57	99.74	98.71	-	-	-	-
Ours	**96.78**	**91.71**	**99.64**	**98.00**	**100**	**99.39**	**94.49**	**85.85**

Celeb-DF dataset and DFDC dataset, to evaluate the generalization ability of our model.

As shown in Tab. 3, it is easy to see that almost all models perform worse on cross-dataset, but we still achieve better results. For example, on the more difficult DFDC dataset, we outperform the recent SOTA methods on both of them. In particular, while training our model on the more compressed FF++c40 dataset, we improve the AUC by 0.46% on the Celeb-DF dataset and by 1.92% on DFDC.

Clearly, in real-world social media scenarios, the repeated dissemination of forged images undergoes a lossy compression process, leading to a loss of image details that conceals artifacts introduced during the forgery, thereby rendering detection more challenging. This is evident in experiments, as the current forgery detection model suffers a severe performance degradation at FF++c40 compared to FF++c23, which involves greater compression.

BAM, motivated by this, is introduced in our model. We believe that through the optimization of weights between different frequency bands learned during training, BAM modulates these bands to partially restore the high-frequency components lost during compression, thus emulating the inverse process of JPEG compression through learning. As a result, there is also less performance degradation in our model when trained on the more compressed FF++c40 dataset compared to FF++c23.

In addition, considering that FF++, Celeb-DF, and DFDC contain many videos of faces, we also evaluate the video-level performance by averaging the scores of the frames. As shown in the Tab. 3, we still achieve good results in the lack of temporal information, which is widely involved in video forgery detection methods, such as FTCN and LipForensics. Our results are only slightly lower than theirs, and achieving this comparable performance without using temporal features shows the strength of our model.

Table 3: Cross-dataset evaluation of the FF++ dataset by AUC (%). FF++c23 and FF++c40 were used as training sets, and Celeb and DFDC were used as testing sets to evaluate the method ability, respectively. The top three results are highlighted in red, green, and blue.

Image-level (IL)				**Image-based Video-Level (IVL)**			
Methods	Training	Testing		Methods	Training	Testing	
		Celeb	DFDC			Celeb	DFDC
SMIL [20]		56.30	-	Two-branch [25]		76.70	-
Add-Net [55]		57.83	51.60	M2TR [45]		72.05	66.02
Xception [33]		65.50	69.70	F^3-Net [31]	FF++	77.92	67.35
M2TR [45]		66.15	70.29	F^2 Trans-B [28]	(C40)	83.96	74.20
PEL [12]	FF++	69.18	63.31	**Ours**		**82.44**	**74.28**
FRLM [27]	(C40)	70.58	69.81	PatchForensics [3]		69.60	65.60
F^3-Net [31]		71.29	65.39	CNN-GRU [47]		69.80	68.90
Two-branch [25]		73.41	-	F^3-Net [31]		75.68	70.88
SPSL [22]		76.68	-	M2TR [45]		75.76	73.12
F^2 Trans-B [28]		77.61	70.39	Xception [33]		73.70	70.90
Ours		**78.74**	**72.42**	GFF [24]		75.31	71.58
F^3-Net [31]		68.69	67.45	STIL [13]	FF++	75.58	-
Xception [33]		65.30	72.20	MADD [51]	(C23)	76.65	67.34
MADD [51]		67.44	-	LTW [37]		77.14	74.58
M2TR [45]	FF++	69.94	69.94	Face X-ray [19]		79.50	65.50
MTD-Net [50]	(C23)	70.12	-	DCL [38]		82.30	76.71
LiSiam [44]		78.21	-	FTCN [54]		86.90	74.00
F^2 Trans-B [28]		83.05	71.81	F^2 Trans-B [28]		89.87	76.15
Ours		**81.85**	**72.37**	**Ours**		**85.85**	**75.51**

Unseen Manipulations Evaluation. In this section, we test the generalization ability of our model against different tampering methods. With the rapid development of technology, there are various ways of forgery, so the robustness of the model against unknown tampering methods is an important issue. Four tampering methods are used in the FF++ dataset, namely DF, FF, FS, and NT. We use different tampering modalities for the training and testing sets, to evaluate the robustness of our model against unknown tampering modalities.

Following the experimental setup of LTW, we conduct a cross-manipulation experiment. We use three tampering methods as the training set and the remaining one as the testing set. For example, GID-DF uses FF, FS, and NT as the training set and DF as the testing set. As shown in Tab. 4, we achieve the highest values in all cases. The experiment demonstrates the robustness of our model against unknown tampering types. Therefore, our model may be more effective than the state-of-the-art method for generalizable deep forgery detection tasks. Our model also holds promise in maintaining competitiveness against new forgery algorithms that may emerge in the future.

Table 4: Cross-manipulation evaluation on the subsets of FF++c40 in terms of AUC(%) and Acc(%). The best results are shown in red. (GID: General Intra-Datasets.)

Methods	GID-DF		GID-FF		GID-FS		GID-NT	
	AUC	Acc	AUC	Acc	AUC	Acc	AUC	Acc
EfficientNet [40]	75.30	67.60	67.40	61.41	-	-	-	-
ForensicTransfer [6]	-	68.20	-	55.00	-	53.00	-	55.00
Multi-task [29]	-	66.76	-	56.50	-	51.70	-	56.00
MLDG [18]	73.12	67.15	61.70	58.12	61.70	58.10	60.70	56.90
LTW [37]	75.60	69.15	72.40	65.70	68.10	62.50	60.80	58.50
DCL [38]	83.82	75.90	75.07	67.85	-	-	-	-
M2TR [45]	84.85	74.29	71.70	66.43	-	-	-	-
F^3 Net [31]	85.77	77.50	73.70	64.64	-	-	-	-
F^2 Trans-B [28]	88.77	82.14	77.73	70.36	-	-	-	-
Ours	**89.91**	**82.86**	**83.23**	**73.93**	**70.46**	**63.93**	**69.48**	**62.50**

4.4 Ablation Study

To enhance validation speed and item discrimination, we perform ablation studies on the FF++c23 dataset. We utilize full-coverage uniform sampling on the testing set adopting a more demanding data partitioning strategy. The following sections detail the ablation studies conducted:

Vanilla, BAM, or FCAM? Without any frequency processing, that is, within our vanilla model, the original images are input directly into 2D-RetNet for feature extraction. The application of BAM applies attention modulation between frequency bands, followed by modulation in the spatial domain after iDCT. Furthermore, we investigate FCAM (Frequency Coefficient Attention Modulation), which is similar to BAM but operates attention granularity at the size of each individual coefficient (224×224) in spectrograms. Theoretically, in terms of asymptotic comparison, FCAM, with finer granularity modulation, should not exhibit inferior expressive capabilities compared to BAM given sufficient training time. However, in empirical non-asymptotic comparison, we observe that within acceptable training overheads, BAM outperforms FCAM and vanilla models slightly on our subset, as depicted in Tab. 5.

Fine-Grained BAM. To better mimic the inverse process of JPEG compression using BAM, images (224×224) are segmented into patches of size 8×8, on which DCT is applied at a finer spatial segmentation granularity. Maintaining a balance of parameter quantity and considering the semantic similarity of patches at similar spatial positions in facial alignment images, we individually train 784 BAM modules for each of the 784 patches of size 8×8. Furthermore, we experiment with Mixed-Grained BAM, applying similar operations to patches of size 16×16 and 32×32, and dynamically adjusting the weights between these resultant attention maps using 1×1-Conv. However, as shown in Tab. 5, these

Table 5: Ablation studies about different frequency attention methods and spatial segmentation granularities, on subsets of FF++c23 in terms of Acc(%) and AUC(%). The best results are shown in red.

Method	vanilla	FCAM	BAM	Fine-Grained BAM	Mixed-Grained BAM
best Acc (%)	94.37	94.93	**95.03**	93.40	94.10
best AUC (%)	98.18	98.09	**98.35**	97.50	98.12

Table 6: Ablation studies about different weight normalization methods and combination methods of GMP and GAP values, on subsets of FF++c23 in terms of Acc(%) and AUC(%). The best results are shown in red.

Method	BAM (Sigmoid, Addition)	Softmax BAM	concatenate BAM
best Acc (%)	**95.03**	94.43	94.80
best AUC (%)	**98.35**	97.94	98.17

methods yield unsatisfactory results in testing on our subset. Also, they significantly increase training consumption.

Other Network Structural Details. In the original CBAM model [48], attention weights are learned by concatenating the features obtained by Global Max-Pooling (GMP) and Global Average-Pooling (GAP), effectively doubling the parameter quantity. Afterward, weights are learned through two fully connected layers, where the hyperparameter *hdim* is usually set to twice the parameter quantity, aiming for thorough mixing of GMP and GAP values to dynamically allocate attention to both the most prominent and average features within the same channel. Although this is initially attempted in BAM, experiments reveal that directly adding GMP and GAP values yields superior results.

On another note, concerning attention weight acquisition, our initial assumption is to use Softmax to compel BAM to consider more targeted strengthening or weakening of certain frequency components. However, experiments also indicate that solely using Sigmoid instead of Softmax to obtain legitimate attention weights is more effective. These aforementioned results are presented in Tab. 6.

5 Conclusions

We propose a face forgery detection method called Bar-Net, which extends RetNet to the 2D structure of an image and fuses the frequency domain information with the RGB information with our newly proposed Band Attention Modulation strategy to extract more hidden features from the image. Numerous experiments demonstrate that our results outperform or are comparable to the state-of-the-art, providing a new way of thinking for image forgery detection.

ACKNOWLEDGMENTS This research was supported by Meituan.

References

1. Afchar, D., Nozick, V., Yamagishi, J., Echizen, I.: Mesonet: a compact facial video forgery detection network. In: 2018 IEEE international workshop on information forensics and security (WIFS). pp. 1–7. IEEE (2018)
2. Bayar, B., Stamm, M.C.: A deep learning approach to universal image manipulation detection using a new convolutional layer. In: Proceedings of the 4th ACM workshop on information hiding and multimedia security. pp. 5–10 (2016)
3. Chai, L., Bau, D., Lim, S.N., Isola, P.: What makes fake images detectable? understanding properties that generalize. In: Computer Vision–ECCV 2020: 16th European Conference, Glasgow, UK, August 23–28, 2020, Proceedings, Part XXVI 16. pp. 103–120. Springer (2020)
4. Choi, Y., Choi, M., Kim, M., Ha, J.W., Kim, S., Choo, J.: Stargan: Unified generative adversarial networks for multi-domain image-to-image translation. In: Proceedings of the IEEE conference on computer vision and pattern recognition. pp. 8789–8797 (2018)
5. Cozzolino, D., Poggi, G., Verdoliva, L.: Recasting residual-based local descriptors as convolutional neural networks: an application to image forgery detection. In: Proceedings of the 5th ACM workshop on information hiding and multimedia security. pp. 159–164 (2017)
6. Cozzolino, D., Thies, J., Rössler, A., Riess, C., Nießner, M., Verdoliva, L.: Forensictransfer: Weakly-supervised domain adaptation for forgery detection. arXiv preprint arXiv:1812.02510 (2018)
7. Dang, H., Liu, F., Stehouwer, J., Liu, X., Jain, A.K.: On the detection of digital face manipulation. In: Proceedings of the IEEE/CVF Conference on Computer Vision and Pattern recognition. pp. 5781–5790 (2020)
8. Dolhansky, B., Bitton, J., Pflaum, B., Lu, J., Howes, R., Wang, M., Ferrer, C.C.: The deepfake detection challenge (dfdc) dataset. arXiv preprint arXiv:2006.07397 (2020)
9. Dosovitskiy, A., Beyer, L., Kolesnikov, A., Weissenborn, D., Zhai, X., Unterthiner, T., Dehghani, M., Minderer, M., Heigold, G., Gelly, S., et al.: An image is worth 16x16 words: Transformers for image recognition at scale. arXiv preprint arXiv:2010.11929 (2020)
10. Fridrich, J., Kodovsky, J.: Rich models for steganalysis of digital images. IEEE Transactions on information Forensics and Security **7**(3), 868–882 (2012)
11. Gao, H., Pei, J., Huang, H.: Progan: Network embedding via proximity generative adversarial network. In: Proceedings of the 25th ACM SIGKDD International Conference on Knowledge Discovery & Data Mining. pp. 1308–1316 (2019)
12. Gu, Q., Chen, S., Yao, T., Chen, Y., Ding, S., Yi, R.: Exploiting fine-grained face forgery clues via progressive enhancement learning. In: Proceedings of the AAAI Conference on Artificial Intelligence. vol. 36, pp. 735–743 (2022)
13. Gu, Z., Chen, Y., Yao, T., Ding, S., Li, J., Huang, F., Ma, L.: Spatiotemporal inconsistency learning for deepfake video detection. In: Proceedings of the 29th ACM international conference on multimedia. pp. 3473–3481 (2021)
14. Haliassos, A., Vougioukas, K., Petridis, S., Pantic, M.: Lips don't lie: A generalisable and robust approach to face forgery detection. In: Proceedings of the IEEE/CVF conference on computer vision and pattern recognition. pp. 5039–5049 (2021)
15. Hernandez-Ortega, J., Tolosana, R., Fierrez, J., Morales, A.: Deepfakes detection based on heart rate estimation: Single-and multi-frame. In: Handbook of Digital

Face Manipulation and Detection: From DeepFakes to Morphing Attacks, pp. 255–273. Springer International Publishing Cham (2022)
16. github I: Deepfaks. [2018-10-29], https://github.com/deepfakes/faceswap/ Accessed October 29, 2018
17. github I: faceswap. [2018-10-29], https://github.com/MarekKowalski/FaceSwap/ / Accessed October 29, 2018
18. Li, D., Yang, Y., Song, Y.Z., Hospedales, T.: Learning to generalize: Meta-learning for domain generalization. In: Proceedings of the AAAI conference on artificial intelligence. vol. 32 (2018)
19. Li, L., Bao, J., Zhang, T., Yang, H., Chen, D., Wen, F., Guo, B.: Face x-ray for more general face forgery detection. In: Proceedings of the IEEE/CVF conference on computer vision and pattern recognition. pp. 5001–5010 (2020)
20. Li, X., Lang, Y., Chen, Y., Mao, X., He, Y., Wang, S., Xue, H., Lu, Q.: Sharp multiple instance learning for deepfake video detection. In: Proceedings of the 28th ACM international conference on multimedia. pp. 1864–1872 (2020)
21. Li, Y., Yang, X., Sun, P., Qi, H., Lyu, S.: Celeb-df: A large-scale challenging dataset for deepfake forensics. In: Proceedings of the IEEE/CVF conference on computer vision and pattern recognition. pp. 3207–3216 (2020)
22. Liu, H., Li, X., Zhou, W., Chen, Y., He, Y., Xue, H., Zhang, W., Yu, N.: Spatial-phase shallow learning: rethinking face forgery detection in frequency domain. In: Proceedings of the IEEE/CVF conference on computer vision and pattern recognition. pp. 772–781 (2021)
23. Liu, Z., Qi, X., Torr, P.H.: Global texture enhancement for fake face detection in the wild. In: Proceedings of the IEEE/CVF conference on computer vision and pattern recognition. pp. 8060–8069 (2020)
24. Luo, Y., Zhang, Y., Yan, J., Liu, W.: Generalizing face forgery detection with high-frequency features. In: Proceedings of the IEEE/CVF conference on computer vision and pattern recognition. pp. 16317–16326 (2021)
25. Masi, I., Killekar, A., Mascarenhas, R.M., Gurudatt, S.P., AbdAlmageed, W.: Two-branch recurrent network for isolating deepfakes in videos. In: Computer Vision–ECCV 2020: 16th European Conference, Glasgow, UK, August 23–28, 2020, Proceedings, Part VII 16. pp. 667–684. Springer (2020)
26. McCloskey, S., Albright, M.: Detecting gan-generated imagery using color cues. arXiv preprint arXiv:1812.08247 (2018)
27. Miao, C., Chu, Q., Li, W., Li, S., Tan, Z., Zhuang, W., Yu, N.: Learning forgery region-aware and id-independent features for face manipulation detection. IEEE Transactions on Biometrics, Behavior, and Identity Science **4**(1), 71–84 (2021)
28. Miao, C., Tan, Z., Chu, Q., Liu, H., Hu, H., Yu, N.: F 2 trans: High-frequency fine-grained transformer for face forgery detection. IEEE Transactions on Information Forensics and Security **18**, 1039–1051 (2023)
29. Nguyen, H.H., Fang, F., Yamagishi, J., Echizen, I.: Multi-task learning for detecting and segmenting manipulated facial images and videos. In: 2019 IEEE 10th international conference on biometrics theory, applications and systems (BTAS). pp. 1–8. IEEE (2019)
30. Nguyen, H.H., Yamagishi, J., Echizen, I.: Capsule-forensics: Using capsule networks to detect forged images and videos. In: ICASSP 2019-2019 IEEE International Conference on Acoustics, Speech and Signal Processing (ICASSP). pp. 2307–2311. IEEE (2019)
31. Qian, Y., Yin, G., Sheng, L., Chen, Z., Shao, J.: Thinking in frequency: Face forgery detection by mining frequency-aware clues. In: European conference on computer vision. pp. 86–103. Springer (2020)

32. Rahmouni, N., Nozick, V., Yamagishi, J., Echizen, I.: Distinguishing computer graphics from natural images using convolution neural networks. In: 2017 IEEE workshop on information forensics and security (WIFS). pp. 1–6. IEEE (2017)
33. Rossler, A., Cozzolino, D., Verdoliva, L., Riess, C., Thies, J., Nießner, M.: Faceforensics++: Learning to detect manipulated facial images. In: Proceedings of the IEEE/CVF international conference on computer vision. pp. 1–11 (2019)
34. Sagonas, C., Antonakos, E., Tzimiropoulos, G., Zafeiriou, S., Pantic, M.: 300 faces in-the-wild challenge: Database and results. Image and vision computing **47**, 3–18 (2016)
35. Shi, Z., Chen, H., Chen, L., Zhang, D.: Discrepancy-guided reconstruction learning for image forgery detection. arXiv preprint arXiv:2304.13349 (2023)
36. Sun, K., Liu, H., Yao, T., Sun, X., Chen, S., Ding, S., Ji, R.: An information theoretic approach for attention-driven face forgery detection. In: European Conference on Computer Vision. pp. 111–127. Springer (2022)
37. Sun, K., Liu, H., Ye, Q., Gao, Y., Liu, J., Shao, L., Ji, R.: Domain general face forgery detection by learning to weight. In: Proceedings of the AAAI conference on artificial intelligence. vol. 35, pp. 2638–2646 (2021)
38. Sun, K., Yao, T., Chen, S., Ding, S., Li, J., Ji, R.: Dual contrastive learning for general face forgery detection. In: Proceedings of the AAAI Conference on Artificial Intelligence. vol. 36, pp. 2316–2324 (2022)
39. Sun, Y., Dong, L., Huang, S., Ma, S., Xia, Y., Xue, J., Wang, J., Wei, F.: Retentive network: A successor to transformer for large language models. arXiv preprint arXiv:2307.08621 (2023)
40. Tan, M., Le, Q.: Efficientnet: Rethinking model scaling for convolutional neural networks. In: International conference on machine learning. pp. 6105–6114. PMLR (2019)
41. Thies, J., Zollhöfer, M., Nießner, M.: Deferred neural rendering: Image synthesis using neural textures. Acm Transactions on Graphics (TOG) **38**(4), 1–12 (2019)
42. Thies, J., Zollhofer, M., Stamminger, M., Theobalt, C., Nießner, M.: Face2face: Real-time face capture and reenactment of rgb videos. In: Proceedings of the IEEE conference on computer vision and pattern recognition. pp. 2387–2395 (2016)
43. Vaswani, A., Shazeer, N., Parmar, N., Uszkoreit, J., Jones, L., Gomez, A.N., Kaiser, Ł., Polosukhin, I.: Attention is all you need. Advances in neural information processing systems **30** (2017)
44. Wang, J., Sun, Y., Tang, J.: Lisiam: Localization invariance siamese network for deepfake detection. IEEE Transactions on Information Forensics and Security **17**, 2425–2436 (2022). https://doi.org/10.1109/TIFS.2022.3186803
45. Wang, J., Wu, Z., Ouyang, W., Han, X., Chen, J., Jiang, Y.G., Li, S.N.: M2tr: Multi-modal multi-scale transformers for deepfake detection. In: Proceedings of the 2022 international conference on multimedia retrieval. pp. 615–623 (2022)
46. Wang, R., Juefei-Xu, F., Ma, L., Xie, X., Huang, Y., Wang, J., Liu, Y.: Fakespotter: A simple yet robust baseline for spotting ai-synthesized fake faces. arXiv preprint arXiv:1909.06122 (2019)
47. Wang, S.Y., Wang, O., Zhang, R., Owens, A., Efros, A.A.: Cnn-generated images are surprisingly easy to spot... for now. In: Proceedings of the IEEE/CVF conference on computer vision and pattern recognition. pp. 8695–8704 (2020)
48. Woo, S., Park, J., Lee, J.Y., Kweon, I.S.: Cbam: Convolutional block attention module. In: Proceedings of the European conference on computer vision (ECCV). pp. 3–19 (2018)

49. Xuan, X., Peng, B., Wang, W., Dong, J.: On the generalization of gan image forensics. In: Chinese conference on biometric recognition. pp. 134–141. Springer (2019)
50. Yang, J., Li, A., Xiao, S., Lu, W., Gao, X.: Mtd-net: learning to detect deepfakes images by multi-scale texture difference. IEEE Transactions on Information Forensics and Security **16**, 4234–4245 (2021)
51. Zhao, H., Zhou, W., Chen, D., Wei, T., Zhang, W., Yu, N.: Multi-attentional deepfake detection. In: Proceedings of the IEEE/CVF conference on computer vision and pattern recognition. pp. 2185–2194 (2021)
52. Zhe, S., Peng, S.: Authentication of splicing manipulation by exposing inconsistency in color shift. Multimedia Tools and Applications **79**(11-12), 8235–8248 (2020)
53. Zheng, Y., Bao, J., Chen, D., Zeng, M., Wen, F.: Exploring temporal coherence for more general video face forgery detection. In: Proceedings of the IEEE/CVF international conference on computer vision. pp. 15044–15054 (2021)
54. Zheng, Y., Bao, J., Chen, D., Zeng, M., Wen, F.: Exploring temporal coherence for more general video face forgery detection. In: Proceedings of the IEEE/CVF international conference on computer vision. pp. 15044–15054 (2021)
55. Zi, B., Chang, M., Chen, J., Ma, X., Jiang, Y.G.: Wilddeepfake: A challenging real-world dataset for deepfake detection. In: Proceedings of the 28th ACM international conference on multimedia. pp. 2382–2390 (2020)